OFFICE OF NAVAL RESEARCH

Contract N00014-91-J-1641

R&T Code 313W001

TECHNICAL REPORT NO. 74

FTIR Study of the Oxidation of Porous Silicon

by

D.B. Mawhinney, J.A. Glass, Jr., and J.T. Yates, Jr.

Submitted To

J. Phys. Chem.

Surface Science Center
Department of Chemistry
University of Pittsburgh
Pittsburgh, PA 15260

14 October 1996

REPORT DOCUMENTATION PAGE

Form Approved
OMB No. 0704-0188

1. AGENCY USE ONLY (Leave blank)	2. REPORT DATE	3. REPORT TYPE AND DATES COVERED
	October 14, 1996	Preprint

4. TITLE AND SUBTITLE

FTIR Study of the Oxidation of Porous Silicon

5. FUNDING NUMBERS

6. AUTHOR(S)

D.B. Mawhinney, J.A. Glass, Jr. and J.T. Yates, Jr.

7. PERFORMING ORGANIZATION NAME(S) AND ADDRESS(ES)

Surface Science Center
Department of Chemistry
University of Pittsburgh
Pittsburgh, PA 15260

8. PERFORMING ORGANIZATION REPORT NUMBER

9. SPONSORING/MONITORING AGENCY NAME(S) AND ADDRESS(ES)

Office of Naval Research
Chemistry Division Code 313
800 North Quincy Street
Arlington, Virginia 22217-5000

10. SPONSORING/MONITORING AGENCY REPORT NUMBER

11. SUPPLEMENTARY NOTES

12a. DISTRIBUTION/AVAILABILITY STATEMENT

12b. DISTRIBUTION CODE

13. ABSTRACT *(Maximum 200 words)*

The oxidation of hydrogen-terminated porous silicon surfaces produced by electrochemical etching has been studied using transmission FTIR spectroscopy. The surface is passivated to oxidation by surface hydrogen below about 523 K. Above this temperature as hydrogen depletion occurs by H_2 evolution, Si surface dangling bond sites, capable of O_2 dissociation, are involved in initiating the first stage of oxidation. Two reactions are observed. The first, O insertion into Si-Si back bonds, leads to O_ySiH_x surface species which exhibit frequency shifts to the blue compared to parent SiH_x stretching modes. In addition, Si-O-Si modes are also observed to form. The second reaction involves oxygen atom insertion into Si-H bonds to produce isolated Si-OH surface species.

14. SUBJECT TERMS

silicon
porous silicon
oxidation
silicon dioxide

15. NUMBER OF PAGES

16. PRICE CODE

17. SECURITY CLASSIFICATION OF REPORT	18. SECURITY CLASSIFICATION OF THIS PAGE	19. SECURITY CLASSIFICATION OF ABSTRACT	20. LIMITATION OF ABSTRACT

Submitted to: J. Phys. Chem.
October 11, 1996

FTIR Study of the Oxidation of Porous Silicon

Douglas B. Mawhinney, John A. Glass, Jr., and John T. Yates, Jr.

Surface Science Center
Department of Chemistry
University of Pittsburgh
Pittsburgh, PA 15260

Abstract

The oxidation of hydrogen-terminated porous silicon surfaces produced by electrochemical etching has been studied using transmission FTIR spectroscopy. The surface is passivated to oxidation by surface hydrogen below about 523 K. Above this temperature as hydrogen depletion occurs by H_2 evolution, Si surface dangling bond sites, capable of O_2 dissociation, are involved in initiating the first stage of oxidation. Two reactions are observed. The first, O insertion into Si-Si back bonds, leads to O_ySiH_x surface species which exhibit frequency shifts to the blue compared to parent SiH_x stretching modes. In addition, Si-O-Si modes are also observed to form. The second reaction involves oxygen atom insertion into Si-H bonds to produce isolated Si-OH surface species.

I. Introduction

The oxidation of silicon has been thoroughly studied on silicon single crystal surfaces[1,2]. Highly controlled silicon dioxide insulating layers are used for barrier junctions in electronic devices as well as for surface passivation in silicon device processing. Vibrational spectroscopic studies of the oxidation process were conducted on silicon single crystals using analytical techniques such as High Resolution Electron Energy Loss Spectroscopy (HREELS)[3] or Internal Reflection Infrared Spectroscopy[4,5]. This investigation focuses on the oxidative behavior of porous silicon, studied by transmission FTIR spectroscopy.

Porous silicon has gained much interest[6-10] since the discovery of its light-emission characteristics[11] under optical and electrical excitation. Controlling the emission wavelength, which is dependent on surface modification[7,12-15] as well as applied bias[14], is a much sought after goal. This ability to control the wavelength output of porous silicon would allow its incorporation into optoelectronic devices such as flat panel displays. Some porous silicon devices have already been demonstrated[16].

Another attractive feature of porous silicon is the enhancement in surface area created by the etching process. Absorption isotherm studies show a surface area of ~200 m^2/cm^3 for porous silicon etched on p-type Si(100)[17]. Given typical porous silicon layer depths of 3-6 μm, a porous layer geometrical area of 1

cm^2, and a site density of 6.8×10^{14} sites/cm^2 for Si(100)[18,19], a new site density of ~10^{18} sites/cm^2 can be calculated for the porous silicon layer.

This gives porous silicon enough surface area to allow surface reactions to be monitored by transmission infrared spectroscopy. This technique not only gives better frequency resolution than HREELS, but also can be used to observe surface reactions at much higher gas pressure than the electron spectroscopies. Because of the random orientation of the porous surface, transmission FTIR is carried out with unpolarized light and does not utilize the selection rules related to the orientation of the surface dipoles.

The focus of earlier research on the oxidation of porous silicon has been on mass changes[20], oxidation under wet conditions[20,21], and the study of the shifting of the Si-H stretching modes[21-23] as oxidation progresses.

This frequency shift has been explained by an induction theory[24,25]. The insertion of more electronegative atoms into silicon backbonds will cause a reduction of the Si-H bond length as the electronegative atom pulls electron density away from silicon and hydrogen. This produces an increase of the bond strength of the Si-H bond, which is caused by an increase of the sigma-character of the Si-H bond. This increase of bond strength associated with sigma bond character results in an increase of the degree of steepness in the potential well walls, which results in an increase in the Si-H stretching frequency. The induction theory has been shown to apply for gas phase molecules[23].

This paper deals with surface modifications due to the oxidation process that are able to be monitored by transmission FTIR spectroscopy. Evidence is presented for the formation of three surface species: (SiOSi), (O_ySiH_x), and (SiOH). Monitoring the formation sequence of these surface species allows the extent of oxidation to be measured. Isotopic studies involving D_2, $^{16}O_2$, and $^{18}O_2$ provide mechanistic information on the oxidation as well as a differentiation between surface and bulk oxide modes.

II. Experimental

A. Vacuum System

The stainless steel gas line system is pumped sequentially with a liquid N_2 cooled zeolite sorption pump, a Pfeiffer-Balzers 50 L/s turbomolecular pump, and a Varian 20 L/s ion pump. The system has a base pressure of $1x10^{-7}$ Torr which can be reached after 20 hours of baking while pumping. The background pressure is measured by both the ion pump current and an ionization gauge. Gas pressures are measured with an MKS capacitance manometer with a range from $1x10^{-3}$ Torr to 1000 Torr. The system is also equipped with a UTI 100C quadrupole mass spectrometer for residual gas analysis and for helium leak detection.

The sample cell used in these experiments is illustrated in Figure 1 and has been described previously[26,27]. The stainless steel cell is used at pressures from

~10^{-8} Torr to ~760 Torr. The sample can be rotated 360° about the vertical axis, allowing it to be moved out of the infrared path for spectral measurement of the background. The sample is held in place by tantalum foil electrical connections that connect via tungsten extensions to a feedthrough. The power leads and type K thermocouple leads pass through a liquid N_2 cooled dewar and connect to a 0-50 A, 0-100 V power supply controlled by a Honeywell UDC 500 digital controller. This setup allows temperature control from 108K to 900K with an accuracy of ± 1K via feedback from the type K thermocouple inserted into a tantalum envelope wedged into a slot on the top of the crystal. The cell is also equipped with differentially pumped KBr infrared windows.

B. Materials

Si(100) p-type, B-doped, 5-10 Ωcm crystals were obtained from Virginia Semiconductors, Inc.. The crystals measured 1.3 cm x 1.3 cm x 0.15 cm thick and were slotted 0.1 cm deep on all four edges to allow insertion of the tantalum electrical connectors and the tantalum envelope which separated the thermocouple from the crystal. All crystals were cleaned by the RCA procedure[28] before the etching process. The crystals were anodically etched in a deoxygenated aqueous solution of 48% HF(aq) and anhydrous ethanol. A dc current of 100 mA was applied with a Hewlett Packard E3612A power supply for 25 seconds to produce a

hydrogenated porous layer of 0.75 cm^2 geometrical area. The etched crystal was dipped in 48% HF(aq) to remove any surface oxide and residual etching solution before being mounted into the infrared cell.

Research grade $^{16}O_2$ with a purity of 99.998% was obtained from Matheson. The gas was transferred directly from the cylinder to the gas line for introduction into the sample cell.

Isotopic oxygen ($^{18}O_2$) was obtained from ICON Services, Inc. The gas had an isotopic purity of 95 atom percent. The gas was transferred from the glass bulb to the gas line for introduction into the sample cell.

D_2 was obtained from Matheson. The gas had an isotopic purity of 99.82 atom percent. The gas was transferred from the glass bulb to the gas line for introduction to the sample cell.

C. IR Measurements

All spectra were measured with a Mattson Research Series I FTIR spectrometer. The spectrometer employed a liquid N_2 cooled HgCdTe detector, sensitive to the infrared region from 4000 - 500cm^{-1}. All spectra were recorded at 2cm^{-1} resolution and averaged using 1024 scans. The spectrometer was controlled from a personal computer using WinFIRST software supplied by Analytical Technology, Inc..

III. Results

A. Porous Silicon Layer Prepared on Si(100)

An infrared spectrum measured at 298K of an unetched Si(100) crystal (Figure 2a) reveals the presence of various silicon crystal modes as well as a Si-O-Si mode at 1108 cm^{-1}. After electrochemical etching (Figure 2b) a number of new absorbances appear in the spectrum. The absorbances at 2141 cm^{-1}, 2115 cm^{-1}, and 2090 cm^{-1} are attributed respectively to $SiH_{x\ (x=3,\ 1,\ 2)}$ stretching modes[29]. At lower wavenumbers, the Si-O-Si absorbance at 1108 cm^{-1} is still present, as well as new features such as the SiH_2 scissor mode at 915 cm^{-1}, and various SiH_x deformation modes overlapping the silicon crystal modes which are observed at 666 cm^{-1}, 622 cm^{-1}, and 615 cm^{-1}. Figure 2c shows the spectral changes produced after heavy oxidation of the porous silicon. New vibrational modes due to Si-OH, O_ySiH_x, and surface Si-O-Si species are observed and will be discussed in more detail later.

B. Partially Oxidized Porous Silicon

The first evidence of oxidation occurs at 523 K under an O_2 pressure of 0.2 Torr, as seen by modification of the frequency of the SiH_x modes. The oxidation

becomes much more evident by 573 K (Figure 3A, spectrum b), as seen by an intensity decrease of the various SiH_x stretching modes, the growth of a broad absorbance band centered at approximately 2160 cm^{-1}, and the development and shift of SiH_x absorbances in the regions near 2254 cm^{-1} and 2199 cm^{-1}. Simultaneously, a broad band near the existing bulk Si-O-Si mode at 1108 cm^{-1} begins to grow with a maximum at 1050 cm^{-1} (not shown), and in the lower frequency regions, the SiH_2 scissor and SiH_x deformation modes begin to diminish in absorbance (not shown). Also, an SiOH absorbance begins to develop at approximately 3736 cm^{-1} with a broad tail extending to lower frequencies (Figure 4).

C. Heavily Oxidized Porous Silicon

As the oxidation proceeds to completion, absorbances develop at 2214 cm^{-1} and 2273 cm^{-1} while the original SiH_x stretching modes disappear completely (Figure 3B). The 3736 cm^{-1} mode increases in intensity (Figure 4), as well as the broad band with a maximum at 1050 cm^{-1} (not shown). At lower frequencies, a new absorbance at 877 cm^{-1} with a shoulder at 841 cm^{-1} appears (not shown). Also, a silicon crystal mode becomes visible again at 615 cm^{-1} as a result of the disappearance of δ (Si-H) modes.

Completing the oxidation process under 760 Torr of O_2 and cooling to 298K leaves new absorbance peaks at 3745 cm^{-1}, 2276 cm^{-1}, 1168 cm^{-1} and 1050 cm^{-1} (Figure 2c), and 881cm^{-1}(Figures 2c and 5). Also present are a silicon crystal mode at 615 cm^{-1} and a bulk Si-O-Si mode at 1108 cm^{-1}.

D. Studies Using Isotopic $^{18}O_2$ and D_2

Oxidation at 650 K performed with 33 Torr of $^{18}O_2$ produced the isotopic mass-affected frequencies, measured at 108K, listed in Table I (Figures 5 and 6).

Oxidation of hydrogenated (H) porous silicon, performed at 650 K with 3 Torr of D_2 and 30 Torr of $^{16}O_2$, showed no evidence of Si-OD formation (Figure 7).

IV. Discussion

A. Spectral Shifts for Silicon Hydride Modes During Oxidation

The oxidation process on hydrogen passivated porous silicon begins near 523 K under an oxygen pressure of 0.2 Torr. This threshold temperature for oxidation is observed by the appearance of oxygen modified hydride stretching modes at higher frequencies compared to those for $SiH_{x\ (x=1-3)}$ species. This

oxidation threshold temperature coincides closely with the hydrogen desorption temperature from porous silicon as reported elsewhere[30], which exposes silicon dangling bonds which can adsorb oxygen.

An induction theory developed to explain the SiH_x shifting phenomenon[24,25] notes that substitution of electronegative atoms into silane causes the hydride stretching modes to shift to higher frequencies. In the case of hydrogenated porous silicon, the general upward frequency shift in the υ (O_ySi-H_x) mode with increasing oxidation is due to an increasing degree of backbonding to oxygen, progressing toward the O_3SiH species. Similar oxidized porous silicon hydride surface species have been proposed by others[3,20-22,31].

The assignment of the 881 cm^{-1} band as an oxidized hydride deformation mode, δ (O_ySiH_x), warrants further discussion because other researchers studying silicon oxidation have assigned absorbances in this region to stretching modes of various oxide species, $Si_xO_{y\ (x=2\text{-}4,\ y=5\text{-}x)}$ [20,32]. However, evidence in favor of our assignment comes from the $^{18}O_2$ oxidation experiment. The resultant shift for the Si-O-Si stretch was ~-50 cm^{-1}; while the 881 cm^{-1} peak shifted only by -5 cm^{-1}. The magnitude of difference between the two shifts can be explained by ^{18}O having a primary isotopic mass effect on the Si-O-Si mode, compared to a secondary mass effect of the same oxygen on the hydride mode.

B. The Formation of Surface Si-O-Si Species

The crystals used in this study contained oxide in the bulk, as evidenced in the 1108 cm^{-1} absorbance in Figure 2a. As oxidation proceeds, a broad absorbance attributed to asymmetric stretching modes of SiO_2 [33,34] begins to appear at frequencies on either side of this bulk mode. The added absorbance grows throughout the oxidation process and eventually covers the region from 1250 cm^{-1} to 950 cm^{-1}, but never merges with the 1108 cm^{-1} band. Also, the 1108 cm^{-1} band fails to shift with $^{18}O_2$ oxidation, showing that it is not related to the surface oxidation process.

Since these two bands never merge they must correspond to two different forms of oxide. The growth of the absorbances in the region from 1250-950 cm^{-1} corresponds to the growth of a layer of amorphous SiO_2, while the 1108 cm^{-1} results from an oxygen atom bound in the bulk of the original silicon crystal. Furthermore, the absence of the broad absorbance features in the 1250-950 cm^{-1} region before oxidation suggests that little surface oxide exists on the electrochemically etched porous silicon surface.

C. The Formation of Various SiOH Species

The various SiOH species have been well studied on silica surfaces[35-38]. The oxidation process on porous silicon creates at least two types of SiOH species, specifically isolated and associated SiOH.

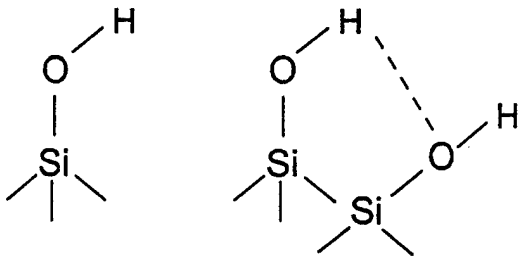

I II and III

The spectral signature for associated Si-OH groups are O-H stretching modes with low frequency compared to those of isolated Si-OH groups due to hydrogen bonding effects[39]. Thus, the spectral development of the SiO-H modes, shown in Figure 4, proceeds from low intensity spectra exhibiting strong relative intensity of associated SiO-H species (~3701 cm^{-1}) to a high intensity spectrum in which most of the SiO-H modes appear to originate from isolated Si-OH groups (~3736 cm^{-1}).

During surface oxidation, a constant initial number of SiH_x species are being converted to O_ySiH_x species and Si-OH species as more and more surface oxide is produce by increased oxidation of the porous silicon as the temperature and exposure to O_2 are increased. The increase in the surface area of SiO_2,

accompanied by a constant initial supply of SiH_x species to produce Si-OH species, would logically lead to the production of an increasing fraction of isolated Si-OH species as oxidation progressed This is in agreement with the changes of the IR spectrum in the SiO-H stretching region as shown in Figure 4.

Three possible routes could lead to the formation of the surface silanol species produced during oxidation, where the equations denote bond character rather than known surface species.

1. Si-O bonds and Si-H bonds react to form the surface silanol:

   $Si\text{-}H + Si\text{-}O \rightarrow SiOH + Si$

2. Water desorbed from the walls of the cell during heating decomposes on the clean silicon surface sites produced above ~523 K[21,40]:

   $H_2O + Si \rightarrow Si\text{-}OH + Si\text{-}H$

3. Desorbing hydrogen reacts with reactant oxygen in the cell to form water. This water then decomposes on the clean silicon surface sites produced above ~523 K.

   $H_2O + Si \rightarrow Si\text{-}OH + Si\text{-}H$

Reaction pathway 2 is disproved by the data from the oxidation experiment with $^{18}O_2$. Vibrational modes due to Si-^{16}OH species would have been observed if this process occurred to a significant extent. However the experiments shown in

Figure 6 indicate that ^{18}O was incorporated into all of the SiOH species on the surface.

A second control experiment disproved reaction pathway 3. Oxidation performed with a D_2 pressure of 3 Torr, showed no SiO-D formation by lack of any vibrational mode in the proximity of 2648 cm^{-1}.

The route to isolated Si-OH species therefore must be related to pathway 1 shown above. At temperatures above about 523 K, SiH_x species begin to decompose producing H_2[30], leaving Si surface dangling bond sites which react with O_2 to produce Si-O bonds. The insertion of O into Si-H bonds then begins to occur, producing Si-OH species which are observed by their characteristic IR spectrum.

V. Conclusions

The oxidation of hydrogenated porous silicon has been studied by transmission FTIR spectroscopy. The following results were obtained:

1. Oxidation occurs at a threshold temperature near 523 K where the first evidence for loss of hydrogen from the surface is observed by IR spectroscopy. The Si dangling bond sites produced are able to chemisorb O_2 dissociatively, leading to the first stage of surface oxidation.

2. Oxidation leads to O insertion into Si-Si backbonds, producing O_ySiH_x species. The Si-H stretching frequencies of these species are characterized by 150-200 cm^{-1} upward frequency shifts compared to SiH_x species as a result of enhanced Si-H sigma bond character caused by electron withdrawal by the oxygen moieties.

3. Oxidation also leads to the formation of surface Si-OH species as a result of O insertion into Si-H bonds. As the degree of oxidation increased, a single SiO-H mode observed near 3736 cm^{-1} develops. This mode is indicative of the formation of isolated Si-OH species, a natural consequence of the limited number of Si-H bonds available in comparison to an increasing number of Si-O-Si bonds produced as oxidation increases.

4. The formation of Si-O-Si modes, originating from oxidation of the porous silicon surface, produces absorbance frequencies near 1176 cm^{-1} and 1065 cm^{-1}. These modes are distinct from Si-O-Si modes at 1134 cm^{-1} and 1125 cm^{-1} which originate from oxygen initially present in the bulk of the silicon.

VI. Acknowledgments

We thank Patrick Maley for his assistance at the beginning of the project and Edward A. Wovchko many useful discussions about the vibrational spectra of silica. We also thank the Office of Naval Research for their support of this work.

Table 1. Observed Frequency Shifts Between $^{16}O_2$ and $^{18}O_2$ Oxidation

	υ (SiO-H)	υ (O_ySiH_x)	υ (Si-O-Si)	υ (Si-O-Si)	δ (O_ySiH_x)
^{16}O	3747 cm^{-1}	2273 cm^{-1}	1176 cm^{-1}	1065 cm^{-1}	881 cm^{-1}
^{18}O	3736 cm^{-1}	2271 cm^{-1}	1121 cm^{-1}	1015 cm^{-1}	876 cm^{-1}

Figure Captions

Figure 1. Drawing of infrared cell containing a porous silicon layer on a silicon (100) single crystal.

Figure 2. Spectra taken at 298K of three different stages of surface modification - a. Silicon (100); b. Porous silicon on Si(100); c. Oxidized porous silicon on Si(100).

Figure 3. A. Early stages of oxidation as noted by development of oxidized silicon-hydride stretching bands. B. Continued growth and shifting of the oxidized silicon-hydride stretching bands as the oxidation temperature is raised.

Figure 4. SiO-H stretching mode development (smoothed data). The reaction conditions for each lettered spectrum corresponds to same conditions as each lettered spectrum in Figure 3 A and B.

Figure 5. Si-O-Si asymmetric stretch, bulk oxide modes, and oxidized silicon-hydride deformation mode measured at 108K after oxidation with $^{16}O_2$ or $^{18}O_2$. The crosshatched absorbance bands indicate the two asymmetric Si-O-Si modes formed by surface oxidation. Fitting was performed with Microcal Origin software. The slight difference in ^{16}O freqencies in the Si-O-Si region here

compared to those seen in Figure 4 are due to temperature differences during the spectral measurements.

Figure 6. Isotopic frequency of the SiO-H stretch after oxidation with $^{18}O_2$, compared to the same mode after $^{16}O_2$ oxidation. The slight difference in ^{16}O freqencies in the isolated SiO-H stretch here compared to those seen in Figure 4 are due to temperature differences during the spectral measurements.

Figure 7. Spectra showing SiO-H stretch and lack of SiO-D stretch after oxidation with 33 Torr $^{16}O_2$ and 3 Torr D_2, demonstrating the absence of D_2O formation and decomposition on the surface.

[1] H. Ibach, K. Horn, R. Dorn, and H. Lüth, Surf. Sci. 38 (1973) 433.

[2] T. Engel, Surf. Sci. Rep. 18 (1993) 91.

[3] J. A. Schaefer, D. Frankel, F. Stucki, W. Gopel, and G. J. Lapeyre, Surf. Sci. 139 (1984) L209.

[4] L. Zazzera and J. F. Evans, J. Vac. Sci. Technol. A, 11 (1993) 934.

[5] M. Niwano, J. Kageyama, K. Kinashi, N. Miyamoto, and K. Honma, J. Vac. Sci. Technol. 12 (1994) 465.

[6] Y. H. Xie, W. L. Wilson, F. M. Ross, J. A. Mucha, E. A. Fitzgerald, J. M. Macaulay, and T. D. Harris, J. Appl. Phys. 71 (1992) 2403.

[7] S. S. Iyer and Y. H. Xie, Science 260 (1993) 40.

[8] L. Canham, MRS Bulletin, July 1993, 22.

[9] S. M. Prokes, J. Mat. Res. 11 (1996) 305.

[10] B. Hamilton, Semiconductor Sci. Tech. 10 (1995) 1187.

[11] L. T. Canham, Appl. Phys. Lett. 57 (1990) 1046.

[12] L. Brus, J. Phys. Chem. 98 (1994) 3575.

[13] S. Wang, W. Z. Shen, X. C. Shen, L. Zhu, Z. M. Ren, Y. F. Li, and K. F. Liu, Appl. Phys. Lett. 67 (1995) 783.

[14] A. Bsiesy, M. A. Hory, F. Gaspard, R. Herino, M. Ligeon, F. Muller, R. Romestain, J. C. Vial, Microelectronic Engineering 28 (1995) 233.

[15] M. A. Tischler, R. T. Collins, J. H. Stathis, and J. C. Tsang, Appl. Phys.

Lett. 60 (1992) 639.

[16] M. Araki, H. Koyama, N. Koshida, Jpn. J. Appl. Phys. Part 1 35 (1996) 1041.

[17] G. Bomchil, R. Herino, K. Barla, and J. C. Pfister, J. Electrochem. Soc. 130(7) (1983) 1611.

[18] C. C. Cheng and J. T. Yates, Jr., Phys. Rev. B 43 (1991) 4041.

[19] Z. H. Lu, K. Griffiths, P. R. Norton, and T. K. Sham, Phys. Rev. Lett. 68 (1992) 1343.

[20] T. Unagami, Jpn. J. Appl. Phys. 19 (1980) 231.

[21] Y. Ogata, H. Niki, T. Sakka, and M. Iwasaki, J. Electrochem. Soc. 142 (1995) 1595.

[22] Y. Kato, T. Ito, and A. Hiraki, Jpn. J. Appl. Phys. 27 (1988) L1406.

[23] P. Gupta, A. C. Dillon, A. S. Bracker, and S. M. George, Surf. Sci. 245 (1991) 360.

[24] G. Lucovsky, Solid State Commun. 29 (1979) 571.

[25] A. Borghesi, G. Guizzetti, A. Sassella, O. Bisi, and L. Pavesi, Solid State Commun. 89 (1994) 615.

[26] P. Basu, T. H. Ballinger, and J. T. Yates, Jr., Rev. Sci. Instrum. 59 (1988) 1321.

[27] J. A. Glass, Jr., E. A. Wovchko, and J. T. Yates, Jr., Surf. Sci. 338 (1995) 125.

[28] W. Kern and D. A. Puotinen, RCA Rev. 31 (1970) 187.

[29] J. A. Glass, Jr., E. A. Wovchko, and J. T. Yates, Jr., Surf. Sci. 338 (1996) 325.

[30] P. Gupta and S. M. George, Phys. Rev. B, 37 (1988) 8234.

[31] C. Morterra and M. J. D. Low, Chem. Comm. (1986) 203.

[32] M. Nakamura, Y. Mochizuki, K. Usami, Y. Ito, and T. Nozaki, Solid State Commun. 50(1984) 1079.

[33] W. Kaiser, P. H. Keck, and C. F. Lange, Phys. Rev. 101 (1956) 1264.

[34] H. J. Hrostowski and R. H. Kaiser, Phys. Rev. 107 (1957) 966.

[35] B. A. Morrow and I. A. Cody, J. Phys. Chem. 77 (1973) 1465.

[36] P. Hoffman and E. Knözinger, Surf. Sci. 188 (1987) 181.

[37] E. A. Wovchko, J. C. Camp, J. A. Glass, Jr., and J. T. Yates, Jr. Langmuir 11 (1995) 2592.

[38] R. K. Iler, *The Chemistry of Silica*; Wiley: New York, 1979.

[39] G. C. Pimentel and A. L. McClellan, *The Hydrogen Bond*; W. H. Freeman and Company: San Francisco, 1960.

[40] X.-L. Zhou, C. R. Flores, and J. M. White, Appl. Surf. Sci. 62 (1992) 223.

IR Cell for Porous Silicon Studies

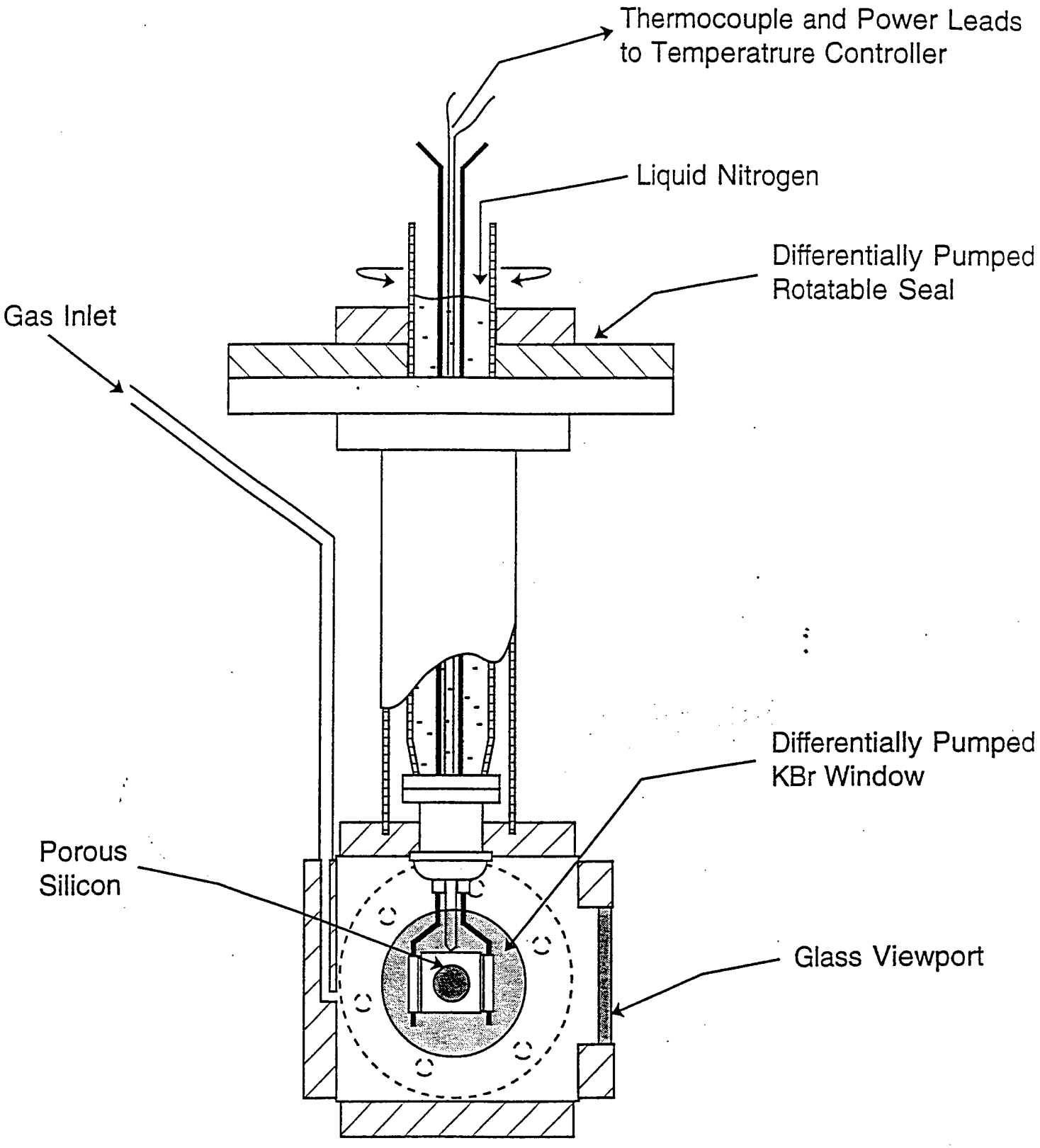

Mawhinney,
et al.

Figure 1

Mawhinney, et al.

Figure 2

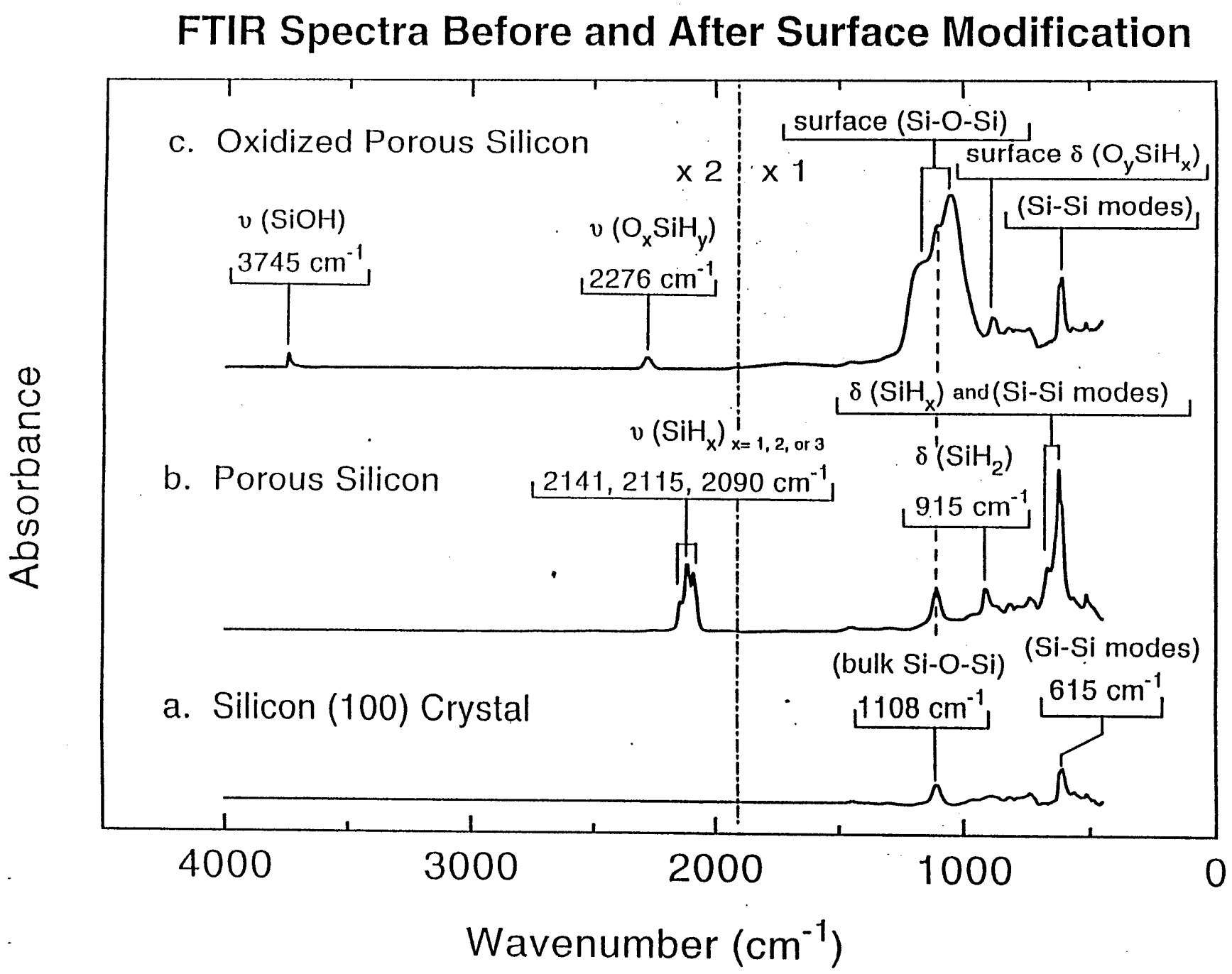

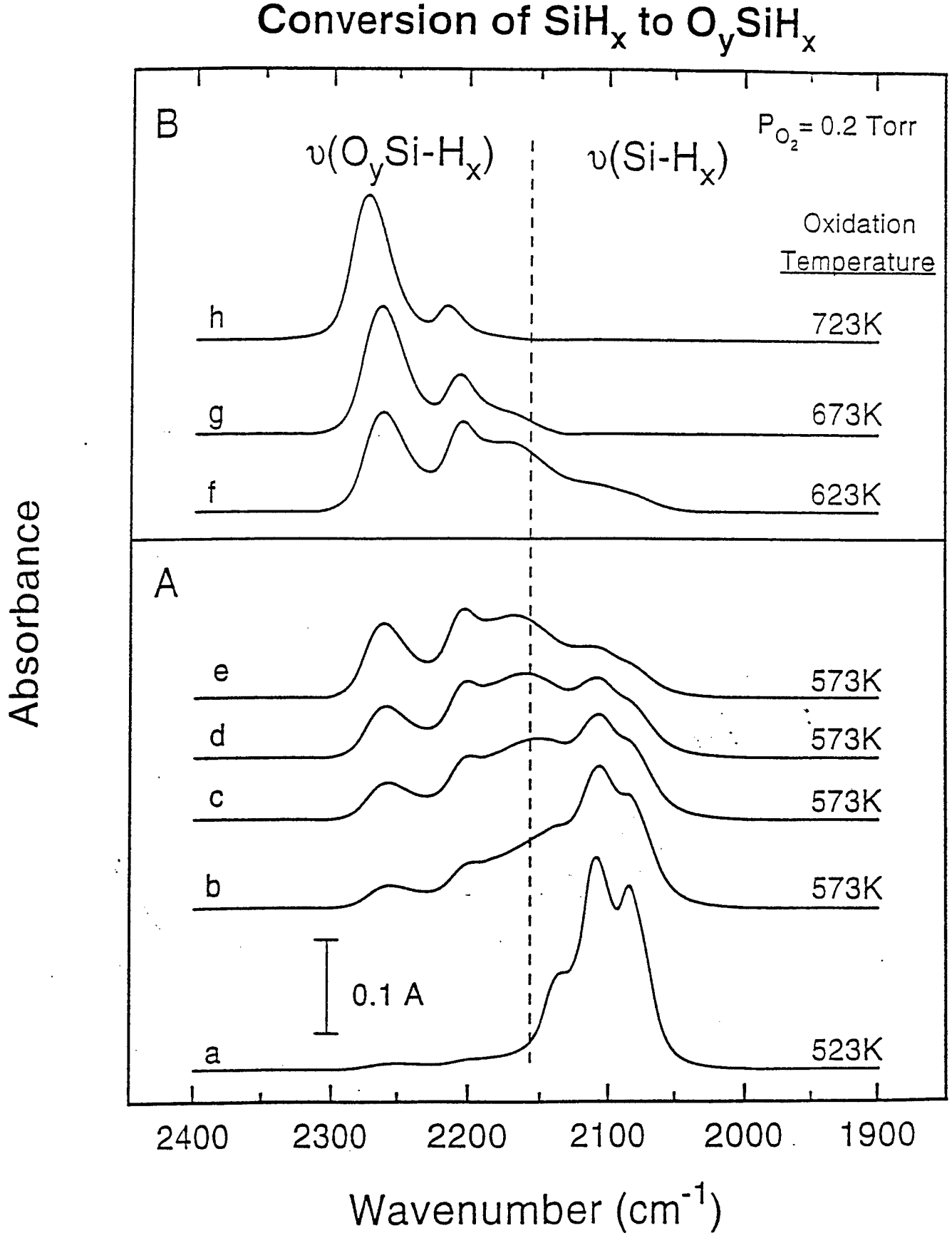

Mawhinney, et al.

Figure 3

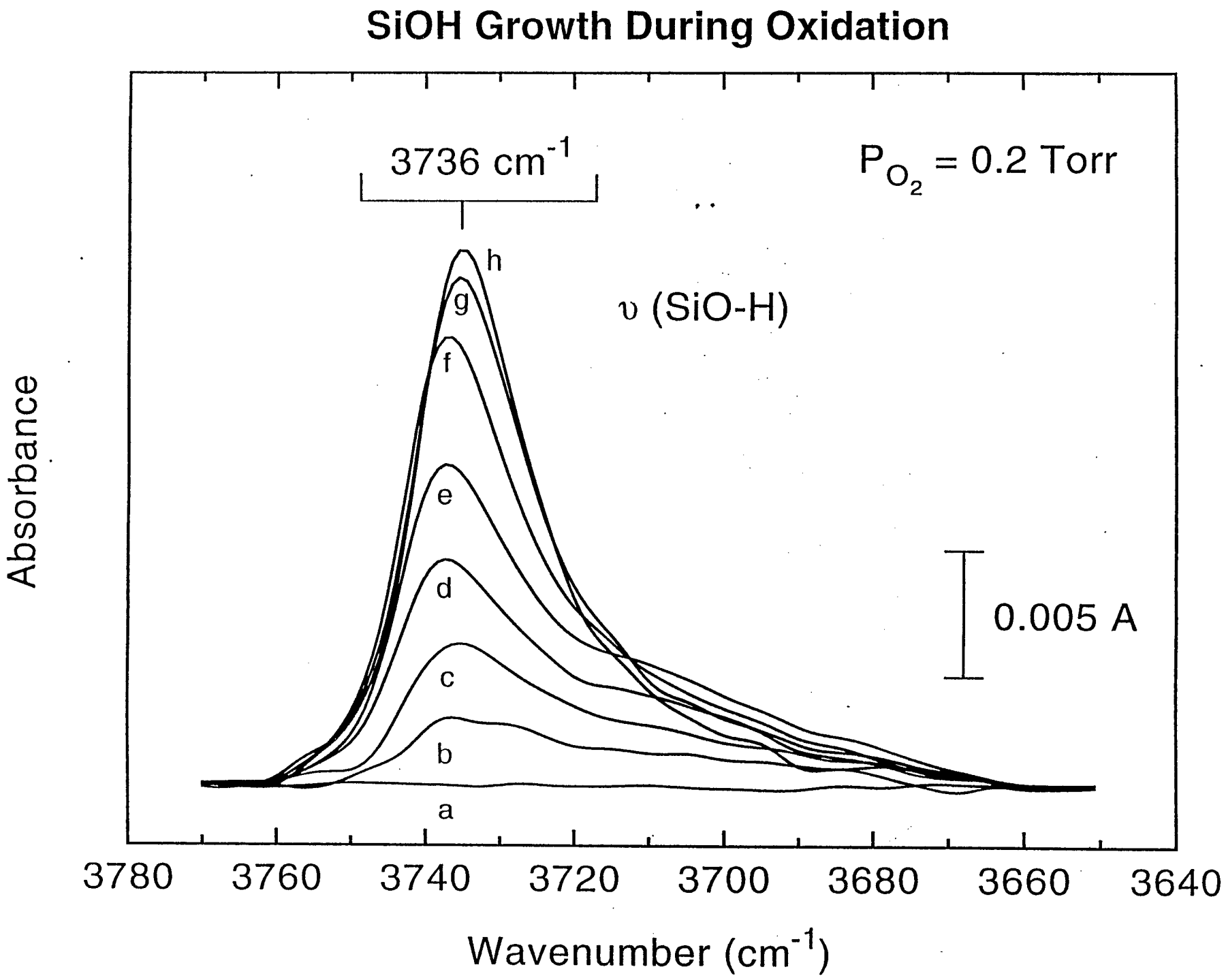
SiOH Growth During Oxidation
3736 cm-1
P O2 = 0.2 Torr
h
g
f
e
d
c
b
a
υ (SiO-H)
0.005 A
Absorbance
3780
3760
3740
3720
3700
3680
3660
3640
Wavenumber (cm-1)

Vibrational Shift Caused by Oxidation With $^{18}O_2$

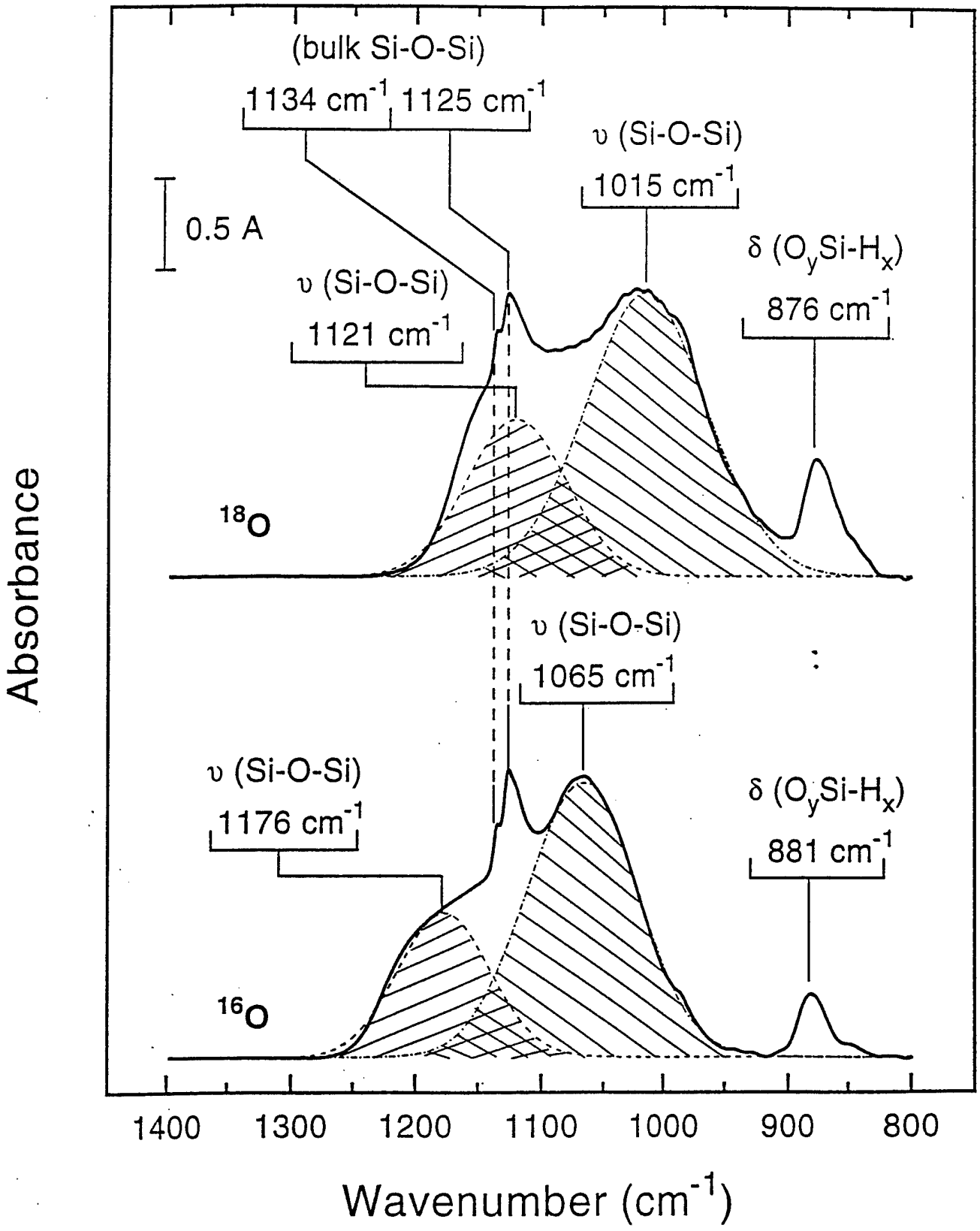

Mawhinney, et al.

Figure 5

Mawhinney, et al.

Figure 6

Vibrational Shift Caused by Oxidation With $^{18}O_2$

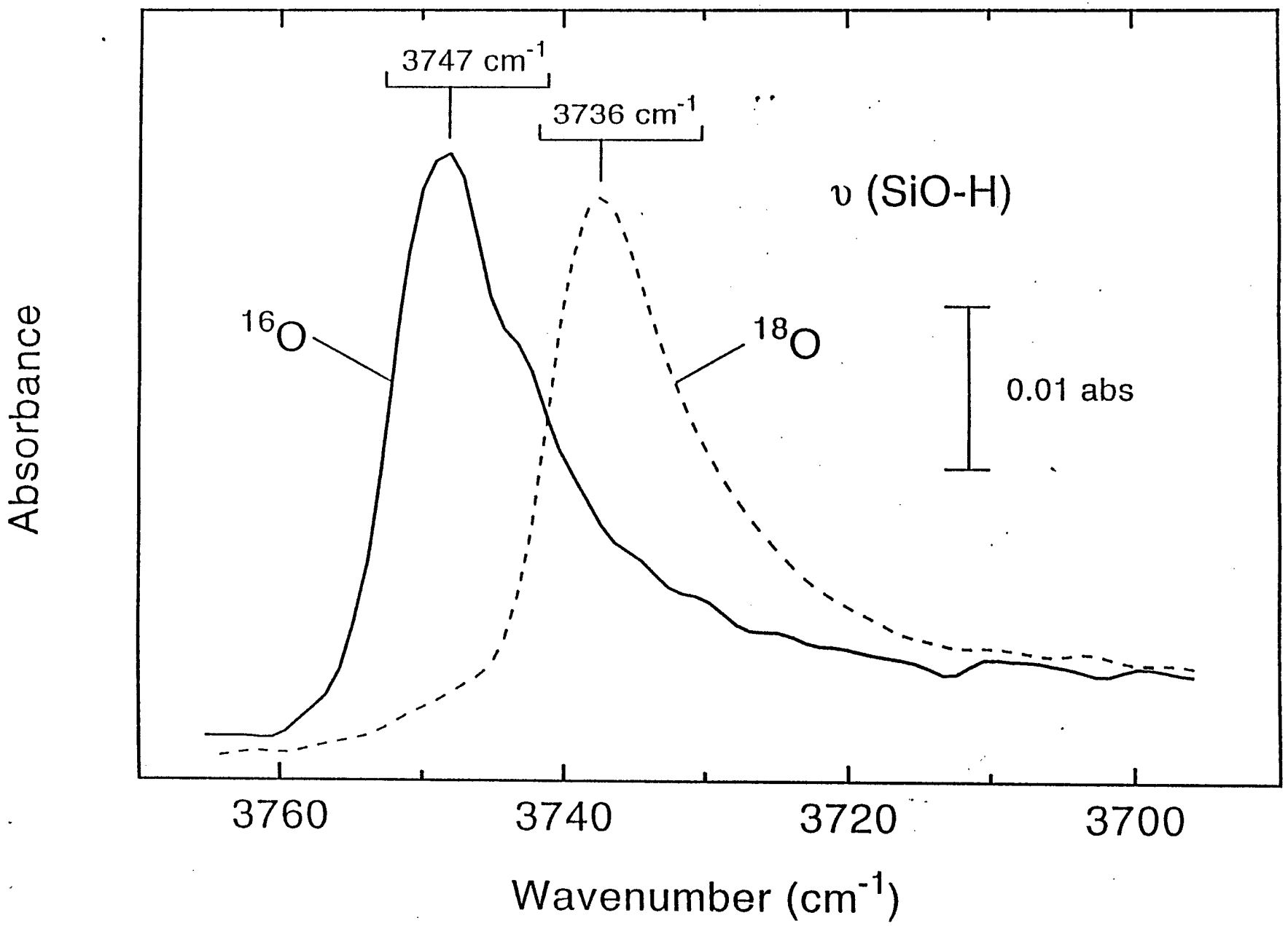

Mawhinney, et al.

Figure 7

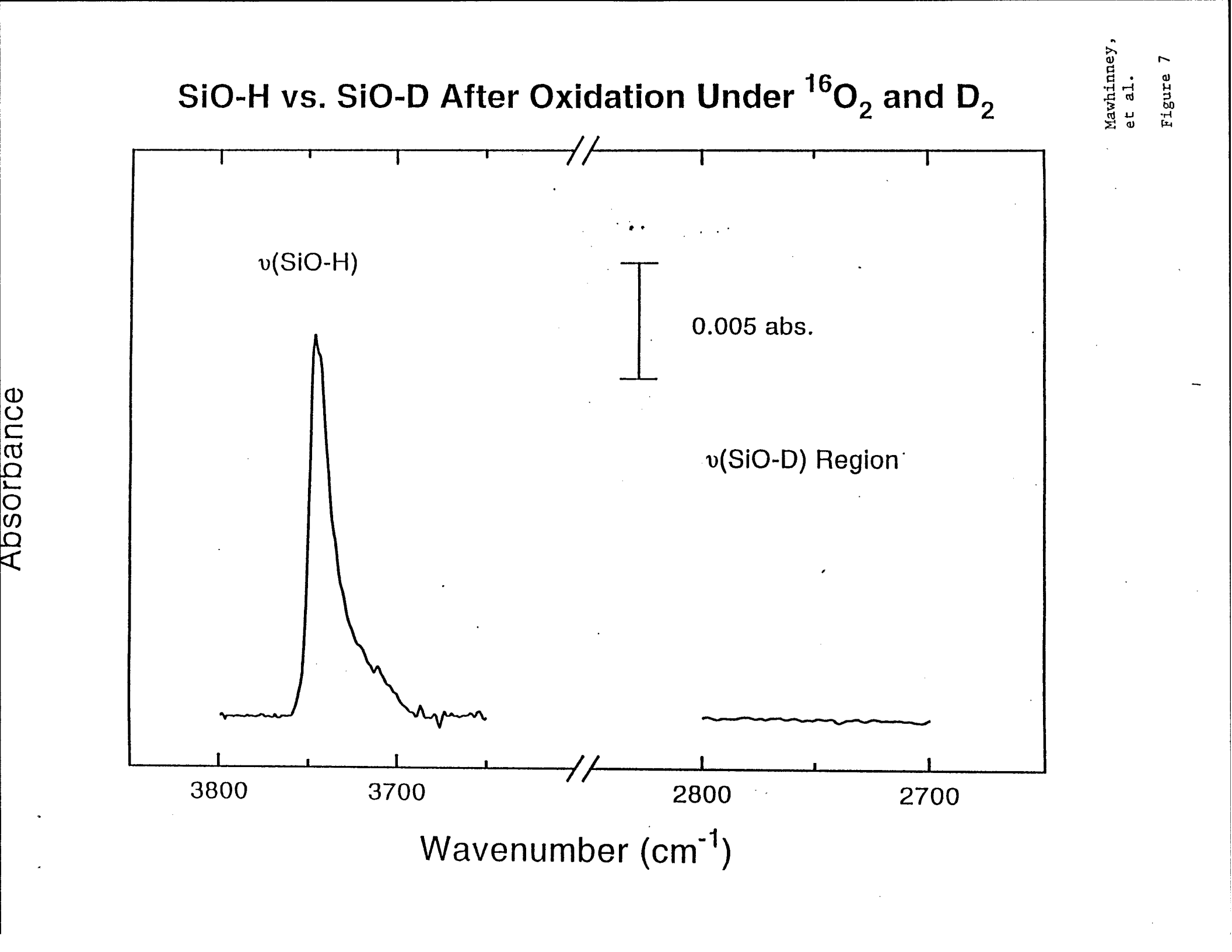

Dr. John C. Pazik (1)*
Physical S&T Division - ONR 331
Office of Naval Research
800 N. Quincy St.
Arlington, VA 22217-5660

Defense Technical Information Ctr (2)
Building 5, Cameron Station
Alexandria, VA 22314

Dr. James S. Murday (1)
Chemistry Division, NRL 6100
Naval Research Laboratory
Washington, DC 20375-5660

Dr. John Fischer (1)
Chemistry Division, Code 385
NAWCWD - China Lake
China Lake, CA 93555-6001

Dr. Peter Seligman (1)
NCCOSC - NRAD
San Diego, CA 92152-5000

Dr. Bernard E. Douda (1)
Crane Division
NAWC
Crane, Indiana 47522-5000

* Number of copies required